ChemComm
Chemical Communications

Accepted Manuscript

This article can be cited before page numbers have been issued, to do this please use: L. Bai, P. Sun, Y. Liu, H. Zhang, W. Hu, W. Zhang, Z. Liu, Q. Fan, L. Li and W. Huang, *Chem. Commun.*, 2019, DOI: 10.1039/C9CC03378E.

ROYAL SOCIETY OF CHEMISTRY

rsc.li/chemcomm

View Article Online
DOI: 10.1039/C9CC03378E

COMMUNICATION

Novel Aza-BODIPY based Small Molecular NIR-II Fluorophores for *in vivo* Imaging

Received 00th January 20xx,
Accepted 00th January 20xx

DOI: 10.1039/x0xx00000x

Lei Bai,[a,†] Pengfei Sun,[b,†] Yi Liu,[a,†] Hang Zhang,[a] Wenbo Hu,[a] Wansu Zhang,[b] Zhipeng Liu,[a,*] Quli Fan,[b,*] Lin Li[a,*] and Wei Huang[a,b,c]

The development of new NIR-II fluorophores, particularly those with facile syntheses, high fluorescence quantum yields, and stable and tunable photophysical properties, is challenging. Herein, we report a new class of small molecular NIR-II fluorophores based on aza-dipyrromethene boron difluoride (aza-BODIPY) dyes. We demonstrate promising photophysical properties of these dyes, such as large Stokes shift, superior photostability, and good fluorescent brightness as nanoparticles in aqueous solution. Because of these properties and high resolution and deep penetration NIR-II imaging ability, aza-BODIPY based dyes show great potential as NIR-II imaging agents.

Biological imaging in the second near-infrared (NIR-II, 1000-1700 nm) window has gained considerable research attention in recent years because of its advantages such as deep tissue penetration, high signal-to-background ratio (SBR), and high maximum permissible exposure to lasers.[1,2] To achieve NIR-II imaging, the highly tunable electronic structures of various inorganic nanomaterials were investigated, leading to the development of materials such as transition-metal sulfide/oxide semiconductors, single-walled carbon nanotubes (SWNTs),[3] quantum dots (QDs),[4,5] and noble and semimetal nanoparticles (NPs).[6-12] In addition, a few organic polymer nanomaterials with narrow bandgap were also developed.[12] However, applications for both inorganic and organic polymer nanomaterials for clinical use are limited because of their unknown long-term toxicity and excretion time.[13-20] Hence, small molecular and biocompatible NIR-II organic fluorescent dyes are desirable for clinical applications. Unfortunately, the design and synthesis of small molecular organic NIR-II fluorophores are challenging. To date, only two types of small molecular NIR-II fluorophores have been reported (Figure 1 and Table S1). One type is based on polymethines. By increasing the conjugation length and heterocycle substitutions, dyes such as **Flav7**, **IR1048**, **IR1061**, **IR26**, and **FD-1080** have shown NIR-II emission and good *in vivo* imaging ability.[21-23] Another type of NIR-II fluorophores is based on benzo[1,2-c:4,5-c0]bis([1,2,5]thiadiazole) (**BBTD**) with a donor-acceptor-donor (**D-A-D**) structure.[24-26] By rational tuning of the electron donating ability of the donor and incorporation of substitutes with good water solubility, Dai and other groups have reported several BBTD-based NIR-II fluorophores, such as **CH1055**.[24] Although these reported NIR-II fluorophores exhibit good photophysical properties, which facilitate their application in biological imaging, novel NIR-II fluorophores especially with facile syntheses, high fluorescence quantum yields (Φ_f), and stable and tunable photophysical properties are still needed.

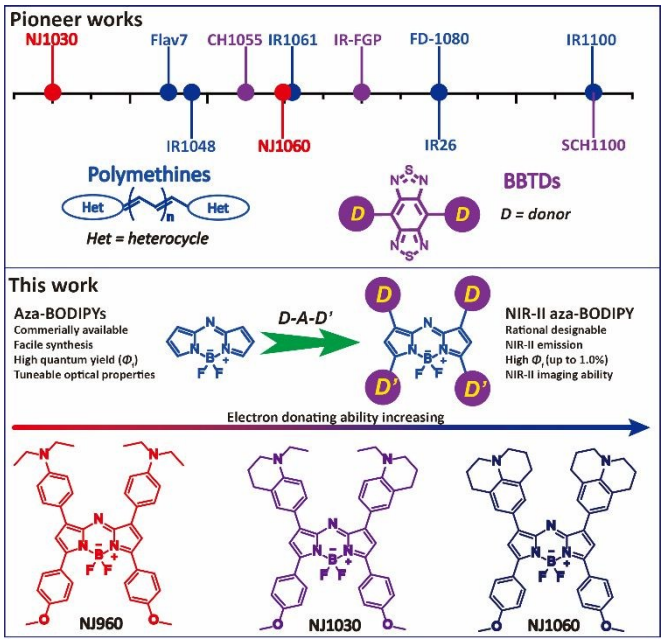

Figure 1. Fluorescence maxima of selected NIR-II dyes and chemical structures of polymethines, **BBTD**s, **NJ960**, **NJ1030**, and **NJ1060**.

Commercially available aza-dipyrromethene boron difluoride (aza-BODIPY) dyes exhibiting favorable NIR-I photophysical properties

[a] *Key Laboratory of Flexible Electronics (KLOFE) & Institute of Advanced Materials (IAM), Nanjing Tech University (NanjingTech), Nanjing 211816, China. iamlli@njtech.edu.cn; iamzpliu@njtech.edu.cn.*
[b] *Key Laboratory for Organic Electronics and Information Displays & Institute of Advanced Materials (IAM), Nanjing University of Posts & Telecommunications, Nanjing 210023, China. iamqlfan@njupt.edu.cn.*
[c] *Shaanxi Institute of Flexible Electronics (SIFE), Northwestern Polytechnical University, 127 West Youyi Road, Xi'an 710072, China.*
† These authors contributed equally.
Electronic Supplementary Information (ESI) available: [details of any supplementary information available should be included here]. See DOI: 10.1039/x0xx00000x

have been investigated for their applications in biological and materials sciences.[27,28] Due to the strong electron-withdrawing nature of borane difluoride azadipyrromethene's center, incorporating electron-donating groups will form a ***D-A*** structure and result in red-shifted absorption and emission.[29-32] For example, O'Shea's group reported that the introduction of the dimethylamino group into the phenyl ring at the 3,5-positions resulted in the distinct red-shift of absorption and emission maxima from 650 and 672 nm to 799 and 823 nm in chloroform solution, respectively.[31] Although the NIR-I absorption and emission properties of aza-BODIPY can be easily achieved *via* facile synthetic derivatization, it is surprising that no aza-BODIPYs with NIR-II emission have been reported. In our efforts to develop new small molecular NIR-II fluorophores, we explored molecular engineering on the classical aza-BODIPY unit to red-shift its emission from the NIR-I to the NIR-II window. A new family of NIR-II fluorophores based on aza-BODIPY (**NJ960**, **NJ1030**, and **NJ1060**) resulted (Figure 1).

NJ960, **NJ1030**, and **NJ1060** with a ***D-A-D'*** structure were designed by incorporating strong electron-donating groups (***D***), such as 4-(*N*, *N*-dimethylamino)phenyl for **NJ960**, 1-ethyl-1,2,3,4-tetrahydroquinolinyl for **NJ1030**, and 4-julolidinyl for **NJ1060**, into the 3, 5-positions of aza-BODIPY. In addition, 4-anisoly groups were introduced into the 1, 2-positions of aza-BODIPY to act as electron-donating groups (***D'***) and potential functional groups. With the help of the strong ***D*** to ***A*** intramolecular charge transfer (ICT) effect, a large emission red-shift from NIR-I to NIR-II for aza-BODIPY is expected compared with that of classical aza-BODIPYs.[27-32] Theoretical calculations were performed to support this prediction. Using time-dependent density functional theory (TD-DFT), calculations based on the optimized ground state in water w/o DMSO (20%) were done. Two main allowed electronic transitions from the highest occupied molecular orbital (HOMO) to the lowest unoccupied molecular orbital (LUMO) and from HOMO-1 to LUMO were observed for **NJ960**, **NJ1030**, and **NJ1060** in the NIR-I region (773 and 641 nm, 796 and 646 nm, and 823 and 666 nm, respectively) (Figure S1-3 and Table S2). The red-shift of the absorption maximum of 773, 796, and 823 nm for **NJ960**, **NJ1030**, and **NJ1060**, can be ascribed to the increasing electron-donating ability of 4-(*N*, *N*-dimethylamino)phenyl, 1-ethyl-1, 2, 3, 4-tetrahydroquinolinyl, and 4-julolidinyl, respectively. The geometries of **NJ1060**, **NJ1030**, and **NJ1060** NPs in the singlet excited state (S_1) were further perfected in water and the excitations based on the S_1 geometry calculated. The TD-DFT calculations indicated an emissive S_1. The calculated emission maxima for **NJ960**, **NJ1030**, and **NJ1060** were 910, 876, and 980 nm, respectively, indicating the potential NIR-II emission of **NJ960**, **NJ1030**, and **NJ1060** (Figure S1-3 and Table 1). In light of these results, **NJ960**, **NJ1030**, and **NJ1060** were facile synthesized using the classical aza-BODIPY synthesis (the synthetic routes are depicted in Scheme S1) strategy. All the compounds were characterized by ^{1}H, ^{13}C NMR, and HRMS.

The photophysical properties of **NJ960**, **NJ1030**, and **NJ1060** were investigated in PBS solution (pH = 7.4) containing 20% DMSO as a co-solvent. As expected, **NJ960**, **NJ1030**, and **NJ1060** showed their major absorption bands in the NIR-I region, i.e., 651 (ε = 55000 mol^{-1} cm^{-1}) and 799 nm (ε = 40000 mol^{-1} cm^{-1}) for **NJ960**, 668 (ε = 38000 mol^{-1} cm^{-1}) and 830 nm (ε = 26000 mol^{-1} cm^{-1}) for **NJ1030**, and 672 (ε =17000 mol^{-1} cm^{-1}) and 910 nm (ε = 170000 mol^{-1} cm^{-1}) for **NJ1060** (Figure 2a). The most exciting result was that the emission maxima (λ_{em}) centered at 960, 1030, and 1060 nm for **NJ960**, **NJ1030**, and **NJ1060**, respectively, successfully reached the NIR-II region (Figure 2b).

Table 1. Emission related energy gaps (eV) and oscillator strengths (f), configurations of the low-lying excited states of **NJ960**, **NJ1030**, and **NJ1060** calculated by TD-DFT/B3LYP/6-31G(d), based on the optimized S_1 state geometries (Water was used as a solvent in the calculations).

Dye	Electronic transition[a]	TDDFT/B3LYP/6-31G(d)			
		E [eV]	λ [nm]	*f*[b]	Orbitals (coefficient)[c]
NJ960	$S_0 \rightarrow S_1$	1.3624	910	0.7328	H–L (0.70727)
NJ1030	$S_0 \rightarrow S_1$	1.4149	876	0.7157	H–L (0.70681)
NJ1060	$S_0 \rightarrow S_1$	1.2654	980	0.7298	H–L (0.70927)

[a] Only S_1 state was considered. [b] Oscillator strength. [c] MOs involved in the transitions. H = HOMO; L = LUMO.

The photophysical properties of these new NIR-II dyes were also investigated in organic solvents having different polarities. As shown in Figure S4 and Table S3, the fluorescence spectra of **NJ960**, **NJ1030**, and **NJ1060** reach further into the NIR-II region as the solvent polarity increases. For example, **NJ960**, **NJ1030**, and **NJ1060** exhibited λ_{em} in DMSO at 989, 1036, 1070 nm, respectively, which were 65, 80, and 81 nm red-shifted relative to those observed in *o*-dichlorobenzene. Based on the Lippert-Mataga plot, the Stokes shift from 123 to 171 nm for **NJ960**, 124 to 182 nm for **NJ1030**, and 133 to 187 nm for **NJ1060** versus the polarity increment demonstrated the ICT nature of **NJ960**, **NJ1030**, and **NJ1060**. The NIR-II emission of **NJ960**, **NJ1030**, and **NJ1060** in both organic solvents and aqueous solutions showed the rationality of the molecular design.

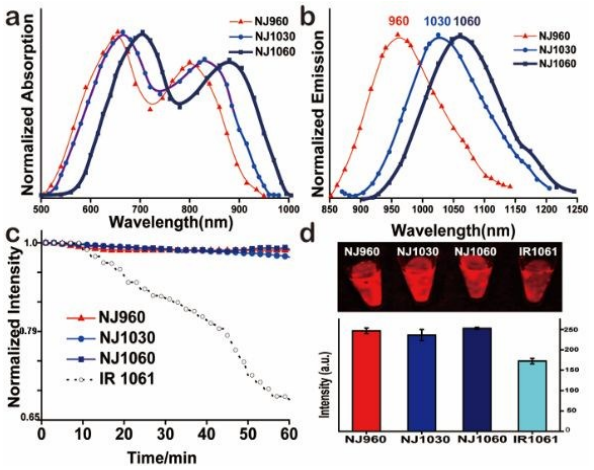

Figure 2. (a) Normalized absorption. (b) Emission spectra of **NJ960**, **NJ1030**, and **NJ1060** in PBS solution (10^{-5} mol L^{-1}). (c) Normalized emission decay of **NJ960**, **NJ1030**, **NJ1060**, and **IR1061** at their emission maxima under laser irradiation (808 nm, 100 mW/cm^2, 60 min) for different irradiation times. (d) **NIR-II f**luorescent images and related emission intensities of **NJ960**, **NJ1030**, **NJ1060,** and **IR1061** in PBS solution at an equivalent absorbance of OD 0.1 at 808 nm.

NJ960, **NJ1030**, and **NJ1060** showed relatively high Φ_f in aqueous solutions. The calculated Φ_f for **NJ960, NJ1030**, and **NJ1060** were 0.16%, 0.2%, and 1.0%, respectively (reference dye **IR 26**, Φ_f = 0.1%), which were slightly higher than those reported for NIR-II fluorophores such as CH1055 and FD-1080 (Table S1). Furthermore, the relative photostability and fluorescent brightness of **NJ960**, **NJ1030**, and **NJ1060** were investigated in PBS solutions containing 20% DMSO as a co-solvent. For comparison, 10 μM concentrations

were tested with **IR1061** tested. After continuous laser irradiation (808 nm, 100 mW/cm^2) for 60 min, the emission intensity of **NJ960**, **NJ1030**, and **NJ1060** remained almost unchanged, while the emission of **IR1061** decayed rapidly from 100% to 65% (Figure 2c). Moreover, the average emission intensity of the imaged vials was 246, 236, and 252 for **NJ960**, **NJ1030**, and **NJ1060**, respectively, which was higher than the 172 for **IR1061** (Figure 2d). These results show the superior photostability and good fluorescent brightness of **NJ960**, **NJ1030**, and **NJ1060.**

Encouraged by the above results, we next investigated the *in vivo* NIR-II imaging ability of **NJ1060** combined with these novel NIR-II dyes. However, due to its low water solubility, **NJ1060** molecules aggregate in water without DMSO as a co-solvent, which means **NJ1060** cannot be used directly for *in vivo* imaging. Hence, **NJ1060** NPs were prepared for *in vivo* NIR-II imaging by using sonication to encapsulate them into a Pluronic F-127 matrix. **NJ1060** NPs, thus, can be homogeneously dispersed in aqueous solutions. **NJ1060** NPs showed spherical morphology with a diameter of ~45 nm, which was characterized by transmission electron microscopy (TEM) (Figure 3a inset). The average diameter of **NJ1060** NPs was measured to be ~90 nm by a dynamic light scattering (DLS) experiment with a low polydispersity index (PDI) of 0.137 (Figure 3a). The smaller diameter observed using TEM was possibly due to shrinking during TEM sample preparation. Most importantly, **NJ1060** NPs showed a maximum absorption at 858 nm and an intense emission peak at 1062 nm, which is consistent with the λ_{abs} (910 nm) and λ_{em} (1060 nm) of molecular **NJ1060** observed in PBS solution (Figure 3b).

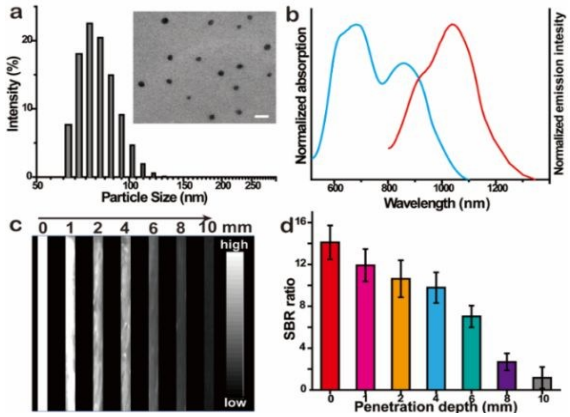

Figure 3. (a) Particle size distribution of **NJ1060** NPs measured by dynamic light scattering with a mean diameter of 90 nm and a PDI of 0.137. Inset: TEM images of **NJ1060** NPs. (b) Normalized absorption and emission spectra of **NJ1060** NPs in PBS solution. (c) NIR-II images of **NJ1060** NPs at different depths (0, 1, 2, 4, 6, 8, and 10 mm). λ_{ex} = 808 nm. (d) SBR ratio of **NJ1060** NPs at different depths.

Before the study of the *in vivo* imaging of **NJ1060** NPs, the NIR-II imaging depth was investigated by imaging a capillary tube filled with **NJ1060** NPs solution within biological tissue (chicken meat) at various depths (Figures 3c and S5). As the depth of imaging increased from 0 to 10 mm, the SBR decreased linearly from 14.1 (0 mm), 10.6 (2 mm), 9.77 (4 mm), 7.0 (6 mm), and 2.68 (8 mm) to 1.2 (10 mm) (Figure 3d). These results show that NIR-II imaging depths for **NJ1060** NPs can reach up to ~8 mm, which is higher than that of other NIR-I imaging agents (~0.2 mm).[3] Moreover, *in vitro* cytotoxicity studies *via* standard XTT analysis showed that no cytotoxicity of **NJ1060** NPs was observed even in concentrations up to 400 μg/mL (Figure S6). All these results suggest that **NJ1060** NPs are applicable for *in vivo* NIR-II imaging applications in living systems.

NIR-II imaging in mice was performed with **NJ1060** NPs. **NJ1060** NPs (c = 0.696 mg/mL, 150 μL) were intravenously injected into mice (n = 3) through the tail vein, then the mice were anesthetized for 5 min before imaging. After irradiating with laser (808 nm), the vasculature of the mouse could be clearly visualized from the surrounding background tissue *via* NIR-II fluorescence (Figures 4a and 4c). For example, according to the full width at half maximum of the emission intensity profiles across the red line of interest, the emission intensities of the hind limb and brain blood vessel resolved by imaging were estimated to be 0.52 and 0.60 mm (Figure 4b and 4d), respectively, which is consistent with previously reported values.[4-12] A comparative imaging experiment was also carried out by using the FDA-approved NIR-I dye indocyanine green (**ICG**, λ_{em} = 835 nm) and classical NIR-II dye **IR1061** (λ_{em} = 1100 nm) as imaging agents. Unfortunately, only the dim fluorescence of both **ICG** and **IR1061** could be observed in whole mice at the same imaging conditions as our experiments, and the vasculature of mice could not be distinguished at all (Figures S7 & S8). These results clearly show the deep penetration and high-resolution imaging ability of the **NJ1060** NPs.

We next investigated the tumor imaging ability of the **NJ1060** NPs (Figure 4e). After intravenous injection of the **NJ1060** NPs through the tail vein into mice (n = 3) with 4T1 tumors at the left shoulder, relatively strong fluorescence was observed in the vasculature and abdomen region. When time was increased to 3 h, the fluorescence signal in the vasculature was reduced accompanied by fluorescence enhancement in the abdomen region. In addition, a weak fluorescence was observed in the tumor. When time was further increased to 6 and 8 h, besides the strong fluorescence in the abdomen, distinct fluorescence enhancement was observed in the tumor, and the SBR increased from 4.9 (1 h) to 23 (8 h), then stabilized at ~30 (24 h) (Figures 4g & S9). This result was attributed to the accumulation of the **NJ1060** NPs through the enhanced permeability and retention (EPR) effect. Furthermore, *ex-vivo* bio-distribution studies showed a high fluorescence intensity in the liver, spleen, and tumor (Figure 4f), demonstrating the preferential accumulation of **NJ1060** NPs in the liver and spleen. These imaging results highlight the great potential for *in vivo* NIR-II imaging of **NJ1060** NPs.

In conclusion, we have developed a new class of small molecular NIR-II dyes (**NJ960**, **NJ1030**, and **NJ1060**) based on the classical aza-BODIPY dye. These dyes were rationally designed under the guidance of theoretical calculations then facile synthesized *via* classical aza-BODIPY synthetic methods. These new aza-BODIPY dyes exhibited NIR-II fluorescence emission with a large Stokes shift, good quantum yield/fluorescent brightness/photostability in aqueous solution, in spite of their low water solubility. The *in vivo* NIR-II imaging results demonstrated the high resolution and deep penetration imaging ability of these dyes with NPs. Considering these results, we can predict that new generations of aza-BODIPY based NIR-II dyes can be developed *via* rational tuning of the **NJ1060** structure. Our future work will focus on the construction of analogues/fluorogenic probes of these new dyes with good water solubility, higher quantum yields, and tunable NIR-II emission wavelengths. We will then investigate their potential uses in clinical applications.

View Article Online
DOI: 10.1039/C9CC03378E

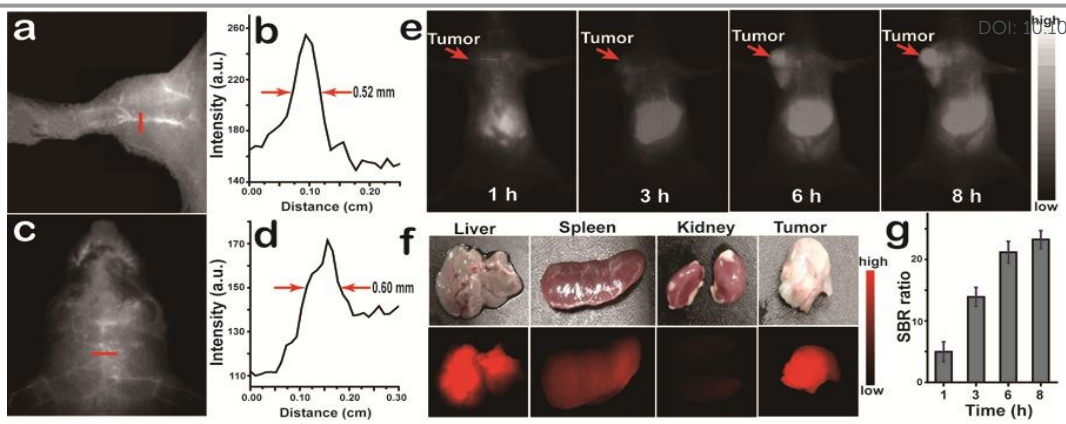

Figure 4. NIR-II images of the mouse hind limb (a) and brain (c) vasculature. The emission intensity profiles of the red line of interest in figure a (b) and figure c (d). (e) The NIR-II images of the 4T1 tumor at different times after tail-vein injection of **NJ1060** NPs under an 808-nm laser excitation. (f) The *ex-vivo* biodistribution of **NJ1060** NPs in the liver, spleen, kidney, and tumor at 4 h under an 808-nm laser excitation. (g) SBR ratios of the tumor at different times.

Conflicts of interest

There are no conflicts to declare.

Acknowledgements

This work was financially supported by the National Natural Science Foundation of China (81672508, 21674048, 21574064 and 21501085), the Jiangsu Provincial Foundation for Distinguished Young Scholars (BK20170041), the Natural Science Foundation of Shaanxi Province (2019JM-016), and the China-Sweden Joint Mobility Project (51811530018).

Notes and references

1 K. Welsher, S. P. Sherlock and H. Dai, *Proc. Natl. Acad. Sci. USA* 2011, **108**, 8943-8948.
2 H. S. Choi, S. L. Gibbs, J. H. Lee, S. H. Kim, Y. Ashitate, F. Liu, H. Hyun, G. Park, Y. Xie, S. Bae, M. Henary and J. V. Frangioni, *Nat. Biotechnol.* 2013, **31**, 148-153.
3 G. Hong, J. C. Lee, J. T. Robinson, U. Raaz, L. Xie, N. F. Huang, J. P. Cooke and H. Dai, *Nat. Med.* 2012, **18**, 1841-1846.
4 O. T. Bruns, T. S. Bischof, D. K. Harris, D. Franke, Y. Shi, L. Riedemann, A. Bartelt, F. B. Jaworski, J. A. Carr, C. J. Rowlands, M. W. B. Wilson, O. Chen, H. Wei, G. W. Hwang, D. M. Montana, I. Coropceanu, O. B. Achorn, J. Kloepper, J. Heeren, P. T. C. So, D. Fukumura, K. F. Jensen, R. K. Jain and M. G. Bawendi, *Nat. Biomed. Eng.* 2017, **1**, 0056.
5 Y. Zhang, G Hong, Y. Zhang, G. Chen, F. Li, H. Dai and Q. Wang, *ACS Nano* 2012, **6**, 3695-3702.
6 R. Wang, L. Zhou, W. Wang, X. Li and F. Zhang, *Nat. Commun.* 2017, **8**, 14702.
7 Y. Zhong, Z. Ma, S. Zhu, J. Yue, M. Zhang, A. L. Antaris, J. Yuan, R. Cui, H. Wan, Y. Zhou, W. Wang, N. F. Huang, J. Luo, Z. Hu and H. Dai, *Nat. Commun.* 2017, **8**, 737.
8 D. J. Naczynski, M. C. Tan, M. Zevon, B. Wall, J. Kohl, A. Kulesa, S. Chen, C. M. Roth, R. E. Riman and P. V. Moghe, *Nat. Commun.* 2013, **4**, 2199.
9 X. Dang, L. Gu, J. Qi, S. Correa, G. Zhang, A. M. Belcher and P. T. Hammond, *Proc. Natl. Acad. Sci. USA* 2016, **113**, 5179-5184.
10 R. Wang, X. Li, L. Zhou and F. Zhang, *Angew. Chem. Int. Ed.* 2014, **53**, 12086-12090.
11 Y. Fan, P. Wang, Y. Lu, R. Wang, L. Zhou, X Zheng, X. Li, J. Piper and F. Zhang, *Nat. Nanotechnol.* 2018, **13**, 941-946.
12 Y. Tang, Y. Li, X. Hu, H. Zhao, Y. Ji, L. Chen, W. Hu, W. Zhang, X. Li, X. Lu, W. Huang and Q. Fan, *Adv. Mater.* 2018, **30**, 1801140.
13 G. Hong, J. T. Robinson, Y. Zhang, S. Diao and A. L. Antaris, *Angew. Chem. Int. Ed.* 2012, **51**, 9818-9821.
14 H. S. Choi, W. Liu, P. Misra, E. Tanaka and J. P. Zimmer, *Nat. Biotechnol.* 2007, **25**, 1165-1170.
15 Z. Liu, C. Davis, W. Cai, L. He and X. Chen, *Proc. Natl. Acad. Sci. USA* 2008, **105**, 1410-1415.
16 A. L. Antaris, J. T. Robinson, O. K. Yaghi, G. Hong, S. Diao, R. Luong and H. Dai. *ACS Nano* 2013, **7**, 3644-3652.
17 K. Welsher, Z. Liu, S. P. Sherlock, J. T. Robinson and Z. Chen, *Nat. Nanotech.* 2009, **4**, 773-780.
18 J. A. J. Fitzpatrick, S. K. Andreko, L. A. Ernst, A. S. Waggoner and B. Ballou, *Nano Lett.* 2009, **9**, 2736-2741.
19 S. T. Yang, X. Wang, G. Jia, Y. Gu and T. Wang, *Toxicol. Lett.* 2008, **181**, 182-189.
20 R. Xie, K. Chen, X. Chen and X. Peng, *Nano Res.* 2008, **1**, 457-464.
21 D. A. Cosco, J. R. Caram, O. T. Bruns, D. Franke, R. A. Day, E. P. Farr, M. G. Bawendi and E. M. Sletten, *Angew. Chem. Int. Ed.* 2017, **56**, 13126-13129.
22 P. Prosposito, M. Casalboni, F. De Matteis, M. Glasbeek, A. Quatela, E. van Veldhoven and H. Zhang, *J. Lumin.* 2001, **94**, 641-644.
23 B. Li, L. Lu, M. Zhao, Z. Lei and F. Zhang, *Angew. Chem. Int. Ed.* 2018, **57**, 7483-7487.
24 A. L. Antaris, H. Chen, K. Cheng, Y. Sun, G. Hong, C. Qu, S. Diao, Z. Deng, X. Hu, B. Zhang, X. Zhang, O. K. Yaghi, Z. R. Alamparambil, X. Hong, Z. Cheng and H. Dai, *Nat. Mater.* 2016, **15**, 235-242.
25 Y. Sun, C. Qu, H. Chen, M. He, C. Tang, K. Shou, S. Hong, M. Yang, Y. Jiang, B. Ding, Y. Xiao, L. Xing, X. Hong and Z. Cheng, *Chem. Sci.* 2016, **7**, 6203-6207.
26 S. Zhua, Q. Yang, A. L. Antaris, J. Yue, Z. Ma, H. Wang, W. Huang, H. Wan, J. Wang, S. Diao, B. Zhang, X. Li, Y. Zhong, K. Yu, G. Hong, J. Luod, Y. Liang and H. Dai, *Proc. Natl. Acad. Sci. USA* 2017, **114**, 962-967.
27 H. Lu, J. Mack, Y. Yang and Z. Shen, *Chem. Soc. Rev.,* 2014, **43**, 4778-4823.
28 Y. Ge and D. F. O'shea, *Chem. Soc. Rev.,* 2016, **45**, 3846-3864.
29 W. Zhao and E. M. Carreira, *Angew. Chem. Int. Ed.* 2005, **44**, 1677-1679.
30 W. Zhao and E. M. Carreira, *Chem. Eur. J.* 2006, **12**, 7254-7263.
31 S. O. McDonnell and D. F. O'Shea, *Org. Lett.,* 2008, **8**, 3493-3496.
32 L. J. Jiao, Y. Y. Wu, S. F. Wang, X. K. Hu, P. Zhang, C. J. Yu, K. B. Cong, Q. L. Meng, E. H. Hao and M. H. J. Vicente, *J. Org. Chem.* 2014, **79**, 1830-1835.